Madridge
Journal of Nanotechnology & Nanoscience

Research Article

Open Access

Frictional Wear Behavior of Ceria Nano-Particles with different Morphologies

Liangbin Hu[1], Changjun Qiu[1]*, Pengfei Hu[1], Zehui Lin[1] and **Yong Chen[1,2]***

[1]*School of Mechanical Engineering, University of South China, Hengyang 421001, China*
[2]*International Iberian Nanotechnology Laboratory (INL), Avenida Mestre Jose Veiga, 4715-330 Braga, Portugal*

Article Info

***Corresponding authors:**
Changjun Qiu
School of Mechanical Engineering
University of South China
Hengyang 421001
China
Tel: +86-734-828-2034
E-mail: qiuchangjun@hotmail.com

Yong Chen
School of Mechanical Engineering
University of South China
Hengyang 421001
China
Tel: +86-734-828-2034
E-mail: chenyongjsnt@163.com

Received: December 20, 2017
Accepted: January 22, 2018
Published: January 27, 2018

Citation: Hu L, Qiu C, Hu P, Lin Z, Chen Y. Frictional wear behavior of Ceria nano-particles with different morphologies. *Madridge J Nanotechnol Nanosci.* 2018; 3(1): 83-86. doi: 10.18689/mjnn-10000115

Abstract

We apply a facile and efficient hydrothermal approach to fabricate four types of cerium nanoparticles, nano-octahedron, cube, rod and sphere. We find that the nanoparticles exhibit marked material removal capacity due to the morphology with well-defined edges, which introduces large contacting stress between the nano-particles CeO_2 slurry and the silicon single crystal substrate. In addition, the frictional wear behavior of the ceria nano-particles with the well-defined edges is found to be of the micro-ploughing wear. The nano-particles with smooth curved surface are found to show good polishing quality in virtue of the abrasive wear mechanism.

Keywords: Hydrothermal process; CeO_2 microstructure; Frictional wear behavior; Morphologies.

Introduction

Ceria (CeO_2) particles have received a great deal of attention recently due to the irremarkable catalytic activity, oxygen sensors, ultraviolet absorbents, polishing performance and so on [1-4]. In particular, sphere-shaped nanoparticles have attracted extensive interest because of their excellent polishing quality [5-11]. Up to now, much effort has been devoted to the controllable synthesis of CeO_2 nanoparticles with a specific size and shape [12-19]. The shape and size of nanocrystals impose significantly impact on their physical and chemical properties [20-22].

The polishing mechanism for CeO_2 spheres is dominated by surface grinding because there is no sharp edge. However, the material removal efficiency of the CeO_2 spheres is rather low. To improve the removal efficiency, the nanoparticles with sharp edge may present preferable cutting ability and hence enhance the material removal efficiency. Here, we fabricated four nanoparticles with different morphologies via a facile hydrothermal process. The morphologies of the CeO_2 nano-particles are characterized by field emission scanning electron microscopy (FE-SEM). Moreover, the polishing properties of the CeO_2nanoparticles at the primary stage of mechanical polishing are investigated.

Experimental

All chemical reagents were of analytical grade (purity: 99.9 wt%, Sigma-Aldrich Co., Ltd) and utilized without further purification. Four specimens with different morphologies (octahedron, cube, rod, and sphere) were synthesized via a facile hydrothermal method no using surfactants and templates. First, cerium nitrate hexahydrate or cerium acetate hydrate was dissolved in distilled water and stirred for15min using a magnetic stirrer. Next, the solution was transferred into autoclaves and treated at a definite temperature at under autogenous pressure. Finally, white products were harvested by centrifuging, washing with distilled water and ethanol to remove unexpected ions, and drying at 343K in air. There

agent and synthesis parameters as follow: ceriumnitrate hexahydrate is 1mmol, K_3PO_4 is 0.01mmol, temperature is 453K,time is 12 h (octahedron); cerium nitrate hexahydrate is 1mmol, KOH is 10 mmol, temperature is 453K, time is 18 h (cube); $Ce(NO_3)_3{\cdot}6H_2O$ is 1mmol, K_3PO_4 is 0.01mmol, H_2O_2 is 6ml, temperature is 503K, time is 24 h, calcinated temperature at 573K,calcinated time is 10h(sphere); cerium acetate hydrate ($Ce(Ac)_3{\cdot}$ nH_2O)is 1mmol,dibasic sodium phosphate (Na_2HPO_4) is 0.01mmol, H_2O_2 is 2 mml (rod).

Octahedron, cube, rod and sphere-shaped nano-particles CeO_2slurry were used for silicon single crystal substrate polishing with a concentration of 1 wt%. In the polishing process, the polishing pad was rotated with a speed of 2000 rpm. During polishing, a constant load of 10 KPa was applied to the polishing head. The polishing time was 1 min.

Microstructures were characterized via the X-ray diffraction (XRD) and scanning electron microscopy (SEM). For the XRD, a Rigaku D/ max-1200X diffractometry with the Cu Kα radiation operated at 45 keV and 200 mA. Morphologies were observed using the Hitachi SU 8000SEM. Microstructures were further observed by transmission electron microscopy (TEM) (JEM-2010F, JEOL) operated at 200 KeV [23-27].

Results and Discussion

To determine the phase of the synthesized particles, XRD analysis was employed as shown in figure 1. Upon a closer indexing, the diffraction peaks of four samples at the angle of 28.5°, 33.1°, 47.5°, 56.3°, 59.1°, 69.4°, 76.7°, 79.1° and 88.4° which could be identified as (111), (200), (220), (311), (222), (400), (331), (420)and(422) lattice planes. No other diffraction peaks were detected by XRD, indicating that the obtained nanoparticles are chemically pure. Hence from the XRD spectra, we could confirm that the four samples which were fabricated via the hydrothermal process are composed of pure fluorite-type ceria without other crystalline impurities.

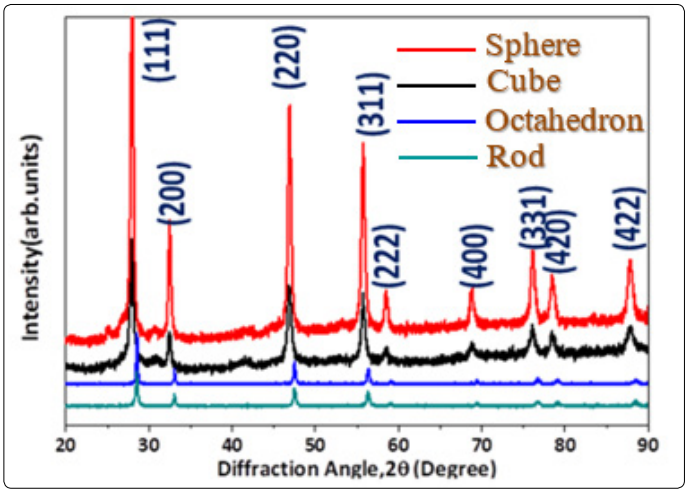

Figure 1. XRD pattern of the CeO_2 samples with different morphologies prepared by hydrothermal method

We carried out SEM to investigate the morphology feature of both as prepared CeO_2 nanostructures. Those CeO_2 nano-octahedron exhibits very sharp corners and edges (Figure. 2(a)). The average size of the nano-octahedrons is estimated to be 100 nm. The figure 2b shows the SEM images of the as-synthesized nanoparticles, from which one can clearly note that the nanoparticles have a cubic shape with sharp corners and well-defined edges. Further, their surfaces are neat and smooth with no other particles adsorbed, the size of the as-synthesized nanoparticles is in principle uniform, ranging slightly from 20 to 44 nm. The uniform sphere particles have an average diameter of about 300nm, and have a crude surface which is covered by wrinkles completely (Figure 2c). Figure 2d presents as-synthesized CeO_2, which reveal a rod-like morphology for the sample. The nano-rods exhibit an average diameter of ~10 nm and an average length of ~400 nm.

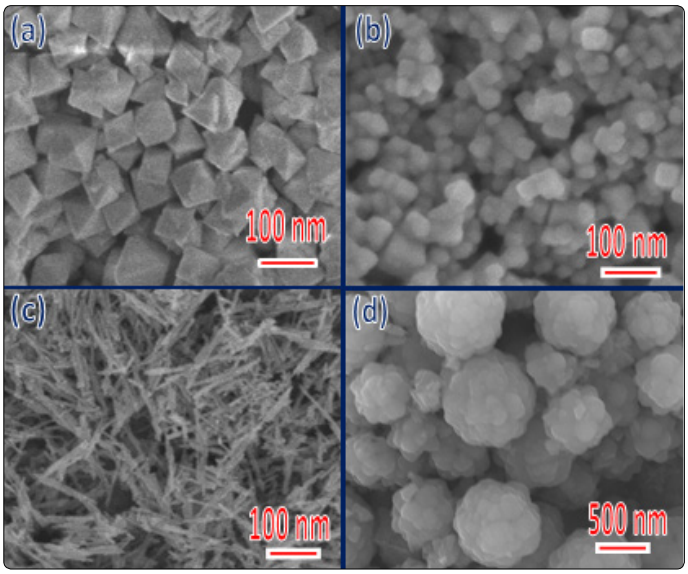

Figure 2. FE-SEM image of (a) octahedrons; (b) cubes; (c) rods; (d) sphere shaped nanoparticles morphologies

To extract microstructure and morphology information of the synthesized CeO_2 nanoparticles, TEM was employed. Fig. 3(a) (d) and (g) show the bright-field TEM images of three typical CeO_2 nanoparticles. Figures 3a and 3b show bright-field TEM images of high crystalline nano octahedrons. The size of the nano-octahedrons is estimated tobe100nm. Figure 3(c) shows typical high-resolution TEM (HRTEM) images taken at a corner of the sample, from which lattice spacing is determined to be~0.31 nm, in line with that of the (111) planes of CeO_2, thereby confirming that the nano-octahedrons is terminated with {111} planes. Figure 3(d), (e) show two typical bright-field images, which confirm that the nanoparticles are of cubic shape and high crystallinity, and that the surfaces are flat and clean. The nano-cubes have an average diameter of ~30 nm. Figure 3 (f) shows a high-resolution TEM (HRTEM) image taken around the corner of a nano-cube. Lattice spacing of two groups of perpendicular lattice fringes is determined to be ~0.27 nm, in accord with that of the CeO_2{001} planes. The nano-rods are uniform with a diameter of ~10 nm and a length of several hundreds of nanometers (Figure 3(g) and (h)). Figure 3 (i) shows an enlarged TEM image of an individual CeO_2 nano-rod, which indicates a prefect crystallinity for the CeO_2 nano-rods. Further selected-area diffraction patterns (SADP) identify the nano-octahedron, nano-cube and nano-rod as face-centered cubic CeO_2 (insert, Figure 3(e), (h) and (i)).

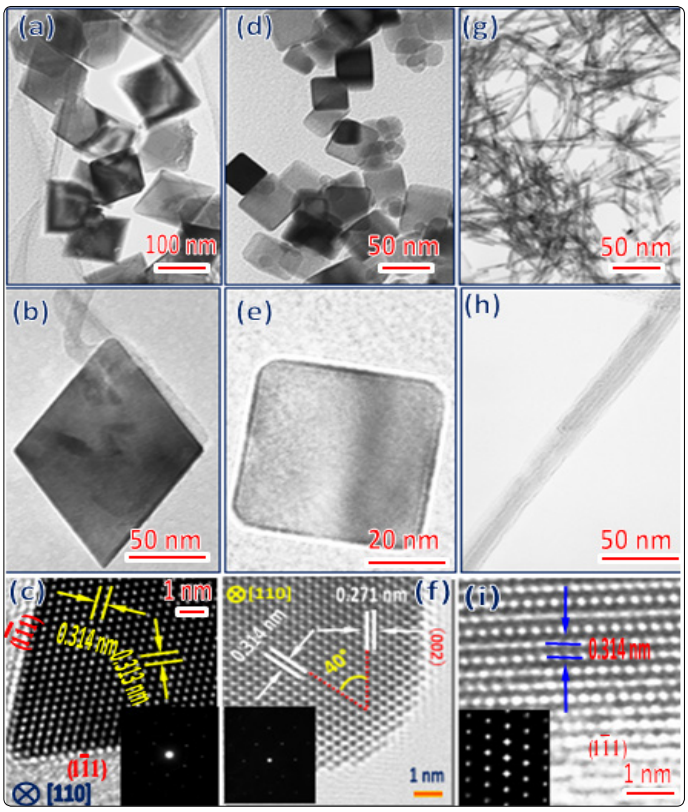

Figure 3. (a) (d) (g) TEM images of the octahedron, cube, rod-shaped CeO_2 nanoparticles. (b), (e), (h) TEM images of the individual nanoparticle with sphere, cube, rod morphologies. (c), (f), (i) HRTEM image of a corner region of the nanoparticles. The inset shows the corresponding SADP identifying each individual nanoparticle.

Figure 4 presents SEM images of the silicon single crystal substrate polished by CeO_2 nanoparticles with different morphologies (octahedron, cube, rod and sphere-shaped). The deep ploughing traces could be detected on the surface of silicon single crystal substrate polished by the octahedron-shaped CeO_2 nanoparticles under a high sliding speed and light-load as shown in figure 4a. From figure 4b, one can confirm that the shadow scratches are found on surfaces of the silicon single crystal substrate due to the rough surface of the sphere-shaped CeO_2 nanoparticles. A small number of slight scratches are observed on surfaces of the silicon single crystal substrate which polished by rod-shaped CeO_2 nanoparticles as show in figure 4c. As can be seen in figure 4d, the furrow scratches are observed on surfaces of the cube-shaped CeO_2 nanoparticles polished silicon single crystal substrate.

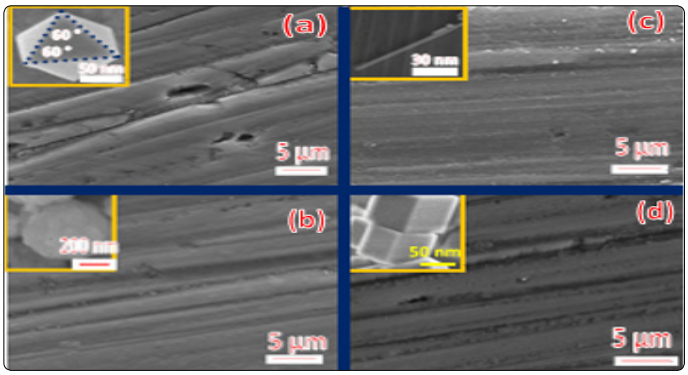

Figure 4. SEM images of the silicon single crystal substrate polished using CeO_2 nanoparticles with different morphologies. The insert shows the corresponding morphologies of polishing CeO_2 nanoparticles.

To shed light on how the interface between the silicon single crystal substrate and CeO_2nanoparticles affect the polish quality and removal efficiency, compressive stress distribution calculations were conducted using the finite element analysis (FEA). The three-dimensional FEA result shows that the compressive stress of the silicon single crystal substrate is 90236 MPa (nano-cube),89730 MPa (nano-octahedron) and 1340.7MPa (nano-spheres)due to the point contact between the CeO_2 nano-particles and silicon substrate (Figures 5c, 5d, and 5g), respectively. While the compressive stress of silicon substrate in case of nano-particles shaped with octahedron and cube are 3681.7 MPa and 2958.5 MPa (Figure 5a and 5e) because the contact method is surface contact. Moreover, the line contact between the octahedron, cube and rod-shaped CeO_2 nano-particles and silicon single crystal substrate could introduce the compressive stress of 23265MPa (nano-cube), 17671 MPa (nano-octahedrons) and 437.42 MPa (nano-rods) (figures 5b,5f and 5h), respectively. Hence, the contact form between CeO_2nano-octahedron and silicon substrate is point contact, which could induce the highest compressive stress.

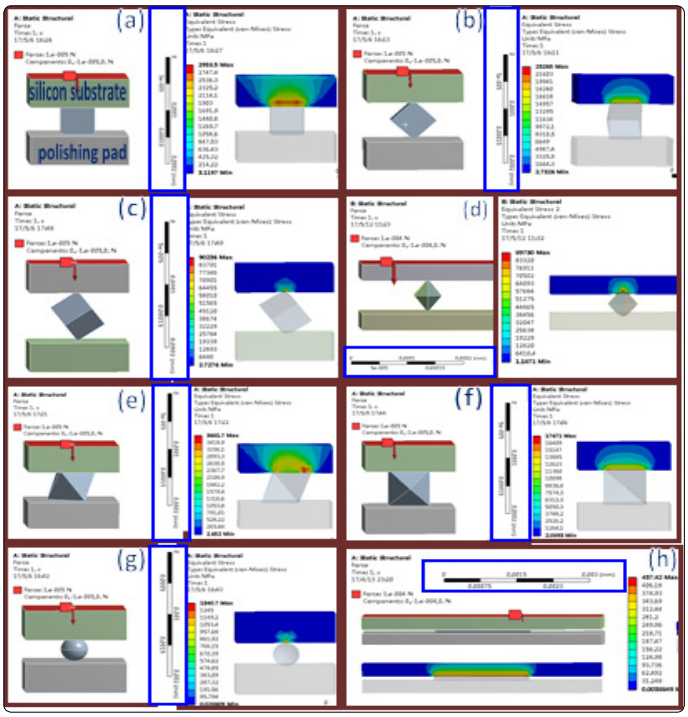

Figure 5. The compressive stress distribution between the silicon single crystal substrate and CeO_2 nanoparticles, which is calculated by the finite element analysis. (a).(b) (c) show the contact form between CeO_2 nano-cube and silicon substrate is surface contact, line contact, point contact respectively. The contact form between CeO_2 nano-octahedron and silicon substrate is (d) surface contact (e) line contact (f) point contact. (g) shows the point contact between CeO_2 nano-sphere and silicon substrate. (h) shows the line contact between CeO_2 nano-rod and silicon substrate.

Since the contact takes the form of point contact, abrasion mechanism of the silicon substrate polished by the sphere-shaped CeO_2 nanoparticles is microscale abrasive wear, while that polished by the nano-octahedron with sharp corners and well-defined edges is micro-ploughing wear [28]. The CeO_2nano-spheres hold improved polishing property, but the material removal rate of silicon surface is lower than that of

CeO_2 nano-octahedron. Conversely, the CeO_2 nano-octahedrons exhibit a stronger material removal capacity and inferior polishing quality than spheres-shaped CeO_2.

Conclusions

We have utilized a facile and efficient hydrothermal method to synthesize four types of ceria nanoparticles, octahedron, cube, rod and sphere-shaped cerium nanoparticles. As a consequence of the unusual morphology, we find that the nanoparticles, i.e.nano-cube and nano-octahedron with well-defined edge scan introduce large stress in contact area between the nano-particles CeO_2 slurry and the silicon single crystal substrate, which can improve markedly material removal capacity due to the micro-ploughing wear behavior. In addition, we also find that the nano-particles with a smooth curved surface can retain the polishing quality for a long time in virtue of the abrasive wear mechanism.

Acknowledgments

Zehui Lin thanks the financial support by the Project of Research Study and Creativity Experiment Plan for College Students of the Hunan province (Hunan Provincial Education Department Bulletingrant no.[2016]283).

References

1. Zhang R, Lu K, Zong L, et al. Gold supported on ceria nanotubes for CO oxidation. *Applied Surface Science*. 2017; 416(Supplement C): 183-190. doi: 10.1016/j.apsusc.2017.04.158
2. Suzuki K, Miyazaki H, Yuzuriha Y, Maru Y, Izu N. Characterization of a novel gas sensor using sintered ceria nanoparticles for hydrogen detection in vacuum conditions. *Sensors and Actuators B: Chemical*. 2017; 250(Supplement C): 617-622. doi: 10.1016/j.snb.2017.05.008
3. Chen Y, Li Z, Miao N. Polymethylmethacrylate (PMMA)/CeO_2 hybrid particles for enhanced chemical mechanical polishing performance. *Tribology International*. 2015; 82(Part A): 211-217.doi: 10.1016/j.triboint.2014.10.013
4. Chen Y, Chen Y, Hu P, Ma S, Li Y. The effects of PVP surfactant in the direct and indirect hydrothermal synthesis processes of ceria nanostructures. *Ceramics International*. 2016; 42(16): 18516-18520. doi: 10.1016/j.ceramint.2016.08.189
5. Liang C, Liu W, Zheng Y, et al. Fractal nature of non-spherical silica particles via facile synthesis for the abrasive particles in chemical mechanical polishing. *Colloids and Surfaces A: Physicochemical and Engineering Aspects*. 2016; 500(Supplement C): 146-153. doi: 10.1016/j.colsurfa.2016.04.031
6. Chen Y, Li Z, Qian C. Core-shell structured polystyrene coated silica composite abrasives with homogeneous shells: The effects of polishing pressure and particle size on oxide-CMP. *Precision Engineering*. 2016; 43(Supplement C): 71-77. doi: 10.1016/j.precisioneng.2015.06.011
7. Suratwala TI, Steele WA, Feit MD, et al. Polishing and local planarization of plastic spherical capsules using tumble finishing. *Applied Surface Science*. 2012; 261(Supplement C): 679-689. doi: 10.1016/j.apsusc.2012.08.081
8. Zhang L, Wang H, Zhang Z, Qin F, Liu W, et al. Preparation of monodisperse polystyrene/silica core-shell nano-composite abrasive with controllable size and its chemical mechanical polishing performance on copper. *Applied Surface Science*. 2011; 258(3): 1217-1224. doi: 10.1016/j.apsusc.2011.09.074
9. Zhang Z, Liu W, Zhu J, Song Z. Synthesis, characterization of ceria-coated silica particles and their chemical mechanical polishing performance on glass substrate. *Applied Surface Science*. 2010; 257(5): 1750-1755. doi: 10.1016/j.apsusc.2010.09.009
10. Feng X, Sayle DC, Wang ZL, et al. Converting ceria polyhedral nanoparticles into single-crystal nanospheres. *Science*. 2010; 312(5779):1504-1508. doi: 10.1126/science.1125767
11. Phuruangrat A, Thongtem S, Thongtem T. Microwave-assisted hydrothermal synthesis and characterization of CeO_2 nanowires for using as a photocatalytic material. *Materials Letters*. 2017; 196(Supplement C): 61-63. doi: 10.1016/j.matlet.2017.03.013
12. Marques TMF, Ferreira OP, da Costa JAP, et al. Study of the growth of CeO_2 nanoparticles onto titanate nanotubes. *Journal of Physics and Chemistry of Solids*. 2015; 87(Supplement C): 213-220. doi: 10.1016/j.jpcs.2015.08.022
13. Xu B, Zhang Q, Yuan S, et al. Synthesis and photocatalytic performance of yttrium-doped CeO_2 with a hollow sphere structure. *Catalysis Today*. 2017; 281(Part 1): 135-143. doi: 10.1016/j.cattod.2016.06.049
14. Cheng C, Chen F, Yi H, Lai G. Large-scale synthesis of highly crystalline rectangular prism-like CeO_2 microrods with excellent lithium storage behavior. *Journal of Alloys and Compounds*. 2017; 694(Supplement C): 276-281. doi: 10.1016/j.jallcom.2016.09.295
15. Choi J, Reddy DA, Islam MJ, Ma R, Kim TK. Self-assembly of CeO_2 nanostructures/reduced graphene oxide composite aerogels for efficient photocatalytic degradation of organic pollutants in water. *Journal of Alloys and Compounds*. 2016; 688(Part B): 527-536. doi: 10.1016/j.jallcom.2016.07.236
16. Wei C, Di Z, Zhang D, et al. Synthesis of modified CeO_2 nanoparticles highly stabilized in organic solvent using higee technology. *Chemical Engineering Journal*. 2016; 304(Supplement C): 573-578. doi: 10.1016/j.cej.2016.07.011
17. Liu H, Liu H. Preparing micro/nano dumbbell-shaped CeO_2 for high performance electrode materials. *Journal of Alloys and Compounds*. 2016; 681(Supplement C): 342-349. doi: 10.1016/j.jallcom.2016.04.207
18. Kim TH, Seon H, Park DW. Synthesis of CeO_2 nanocrystalline powders using DC non-transferred thermal plasma at atmospheric pressure. *Advanced Powder Technology*. 2016; 27(5): 2012-2018. doi: 10.1016/j.apt.2016.07.008
19. Zhang Y, Shi R, Yang P, et al. Fabrication of electronspun porous CeO_2 nanofibers with large surface area for pollutants removal. *Ceramics International*. 2016; 42(12): 14028-14035. doi: 10.1016/j.ceramint.2016.06.009
20. Liu H, Liu H. Preparing micro/nano core–shell sphere CeO_2 via a low temperature route for improved lithium storage performance. *Materials Letters*. 2016; 168(Supplement C): 80-82. doi: 10.1016/j.matlet.2016.01.029
21. He D, Wan G, Hao H, et al. Microwave-assisted rapid synthesis of CeO_2 nanoparticles and its desulfurization processes for CH_3SH catalytic decomposition. *Chemical Engineering Journal*. 2016; 289(Supplement C): 161-169. doi: 10.1016/j.cej.2015.12.103
22. Zhang W, Chen D. Preparation and performance of CeO_2 hollow spheres and nanoparticles. *Journal of Rare Earths*. 2016; 34(3): 295-299. doi:10.1016/S1002-0721(16)60028-5
23. Wang Z, Saito M, McKenna KP, et al. Atom-resolved imaging of ordered defect superstructures at individual grain boundaries. *Nature*. 2011; 479(7373): 380-383. doi: 10.1038/nature10593
24. Li Y, Wang Z, Yao J, et al. Magnetoelectric quasi-(0-3) nanocomposite heterostructures. *Nat Commun*. 2015; 6:6680. doi: 10.1038/ncomms7680
25. Li T, Zeng W, Long H, Wang Z. Nanosheet-assembled hierarchical SnO2 nanostructures for efficient gas-sensing applications. *Sensors and Actuators B: Chemical*. 2016; 231:120-128. doi: 10.1016/j.snb.2016.03.003
26. Wang Z, Zeng W, Gu L, et al. Atomic-scale structure and electronic property of the LaAlO3/TiO2 interface. *Journal of Applied Physics*. 2010; 108(11): 113701. doi: 10.1063/1.3516496
27. Harsha AP, Tewari US. Two-body and three-body abrasive wear behaviour of polyaryletherketone composites. *Polymer Testing*. 2003; 22(4): 403-418. doi: 10.1016/s0142-9418(02)00121-6
28. Long H, Zeng W, Wang H, et al. Self-Assembled Biomolecular 1D Nanostructures for Aqueous Sodium-Ion Battery. *adv. sci*. 2018; 1700634. doi: 10.1002/advs.201700634